

Electrochemical Synthesis of In_2Se_3 Thin Films from Citrate Bath. Structural, Optical and Morphological Investigations

Oualid Dilmi^{a, *} and Mohamed Benaicha^{a, **}

^a Energetic and Solid State Electrochemistry Laboratory, Ferhat Abbas-Setif 1 University, Setif, 19000 Algeria

*e-mail: O.dilmi@univ-jijel.dz

**e-mail: mdbenaicha@univ-setif.dz

Received April 26, 2020; revised August 10, 2020; accepted August 31, 2020

Abstract—In this work, indium selenide In_2Se_3 thin films were synthesized by electrodeposition in potentiostatic mode from aqueous solution containing InCl_3 and SeO_2 in acid medium (pH 4.2) with sodium citrate as complexing agent at ambient temperature with heat treatment of electrodeposited films at different temperatures. Voltammetry method was used to investigate the electrochemical behavior of the electrodeposition bath. The structural characterization of elaborate films was performed by X-rays diffraction (XRD) and Raman spectroscopy, the morphological one was carried out by scanning electron microscopy (SEM) and atomic force microscopy (AFM), the UV–Visible spectrophotometry was used to investigate their optical properties, whereas the Mott–Schottky measurement was used also to study their semiconducting properties. The results showed that the annealed deposit at 350, 450°C and the as-deposited films take the rhombohedral β -crystalline phase hR5 of In_2Se_3 , as-deposited and annealed In_2Se_3 are photoactive thin films with band-gap energies 1.33, 1.55 eV respectively and belong to n-type semiconductors with number of charge carriers in order of $10^{21}/\text{cm}^3$. The obtained deposits have nanometric grain size and less roughness surface.

Keywords: electrodeposition, In_2Se_3 , thin film, citrate bath, semiconductor, energy gap

DOI: 10.1134/S1023193521050049

INTRODUCTION

In_2Se_3 is a photoactive binary compound; it has received great interest in recent years for applications in photovoltaic and photoelectrochemical devices [1–5]. It may consist of at least five significant phases, including the layered structure (α -phase), rhombohedral structure (β -phase), defect wurtzite structure (γ -phase), anisotropic structure (κ -phase) and high temperature phase (δ -phase) [6, 7]. The In_2Se_3 thin films can be obtained by a large number of techniques [8–15], among them the electrodeposition method [16, 17]. The electrodeposition process of thin films is considered as one of the promising ways due to the ability to control the thickness, a large-area deposition, a simple process, good adhesion, reproducible and a low cost fabrication process [18, 19]. Several researchers have used the electrodeposition method to make electroplated In_2Se_3 [16, 17, 20–22]. However, this still requires a broader study and detailed discussion. Among the biggest problems that we face sometimes during the electrodeposition process, the adherence problem; which depends on several factors, among them, the grain size. The deposits with large germs are not suitable in electroplating because the lack of cohesion between them and the little covering of the substrate surface, whereas the deposits with

small germs have a good adherence owing to the good cohesion between their germs. For this reason we must study the electrodeposition process and the deposit morphology in more detail to elucidate the factors and the conditions that facilitate obtaining In_2Se_3 alloys with small germs by optimal methods to meet the requirements of the nanomanufacturing and the nanotechnology industry on the one hand and to strengthen the adherence of the deposited films on the other hand. In this paper, indium selenide In_2Se_3 thin films were synthesized by electrodeposition method from an aqueous solution containing selenium dioxide SeO_2 and indium trichloride InCl_3 in acid medium with sodium citrate as complexing agent which serves to approximate the deposition potentials of selenium and indium ions in order to get electrodeposited alloys. The grain size, the energy gap, the flat band potential and the concentration of free carrier were also investigated.

EXPERIMENTAL

Stationary electrochemical measurements were performed by a system Voltalab PGZ 301 controlled by a computer (software VoltaMaster 4) with a cell of three-electrodes. The saturated calomel electrode (SCE) was used as a reference electrode, the platinum

wire as counter electrode; the indium tin oxide coated glass (ITO) in the form of rectangular sheets was used as work electrode and substrate for the electrodeposition. These substrates were first cleaned in acetone for 5 min, in the nitric acid (30%) during 2 min and finally well rinsed with distilled water.

In this study, all electrochemical experiments were carried out at room temperature using an aqueous solution containing (50 mM) of selenium dioxide (SeO₂), (30 mM) of indium trichloride (InCl₃) and (0.25 M) sodium citrate as complexing agent with pH 4.2 which was adjusted by the addition of some drops of hydrochloric acid (HCl). The heat treatment of obtained films was performed during 20 min under 5×10^{-6} mbar vacuum, the samples were put into a quartz tube connected to a high speed vacuum pump (Adixen-Pfeiffer, Germany). The tube was then introduced into a horizontal tube furnace (Thermolyne-Model 21100) with automatic temperature control accuracy. After annealing, the specimens were cooled down naturally. X-rays diffraction (XRD) measurements were carried out using a Bruker D8 Advance diffractometer with CuK_α radiation (1.5406 Å). The surface morphology of electrodeposited films was investigated using a JSM-6360 SEM. Raman spectrums were obtained using renishaw inVia Raman microscope with a wavelength of 630 nm. The UV-VIS transmittance spectrums have been recorded with a Shimadzu UV-1800 UV-visible Scanning Spectrophotometer. The semiconducting properties were studied using the Mott-Schottky measurements in (0.1 M) KCl aqueous solution with 0.5 kHz employed frequency. Surface roughness of the obtained deposits was studied by AFM MFP 3D Asylum Research.

RESULTANTS AND DISCUSSION

Voltammetry method was performed in order to identify the presence of the electrodeposition processes and to verify the electrochemical behavior of the electrode in the electrodeposition bath. Figure 1 shows a linear voltamogram (cathodic part) of the ITO electrode in our bath traced with a scan rate of 5 mV s⁻¹. As seen, this curve has two cathodic peaks C₁, and C₂ located at 0.9, 1.61 V vs. SCE respectively, it is clear that the peak C₁ related to formation of elemental selenium (Se), whereas peak C₂ relative to the reduction of indium ions in metallic indium (In) according to equations (1) and (2) [16, 23, 24]. In the same curve, we can also see a very small peak at -0.63 V vs. SCE, which can relate to reduction of an impurity ion, as well as the presence of cathodic bearing at about -1.19 V vs. SCE relate probably to formation an InSe alloy i.e. that there is an as-deposition. At -1.68 V vs. SCE in the vicinity of peak C₂ another peak observed

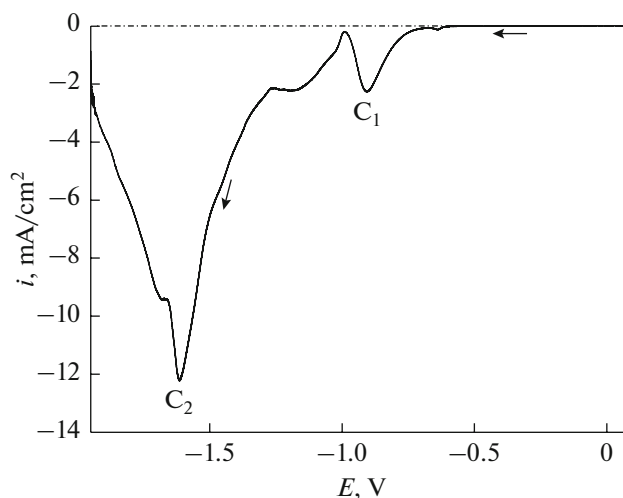
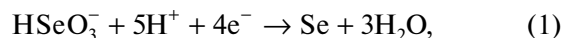
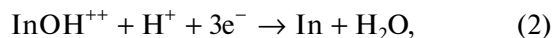


Fig. 1. Voltammogram obtained on the indium tin oxide electrode (ITO) in (0.25 M sodium citrates + 30 mM InCl₃ + 50 mM SeO₂) aqueous solutions with scan rate 5 mV s⁻¹.

which can relate to the irreversible reduction of tin oxide SnO₂ [25].



$$E^0 = 0.778 - 0.0739\text{pH} + 0.0148 \log [\text{HSeO}_3^-],$$



$$E^0 = -0.266 - 0.0197\text{pH} + 0.0197 \log \text{InOH}^{++}.$$

Figure 2 shows X-rays diffraction (XRD) diagram of electrodeposited InSe alloy prepared on ITO substrate at -1.3 V vs. SCE in potentiostatic mode during 10 min and annealed at different temperatures; 350, 450°C and untreated sample as a witness. Using the match program, the obtained peaks were defined by comparing them to the database; we have found that the dominant phase is rhombohedral β-In₂Se₃ crystalline structure hR5 (space group R-3m (166)) for peaks marked with asterisk as shown in the figure [26]. According to the software database; other crystalline phases of electrodeposited InSe alloy were formed also during the electrodepositing process as the hexagonal β-In₂Se₃ hP160 (space group p63 (173)) which corresponds the peaks marked by x symbol and the rhombohedral InSe hR4 (space group R-3m (160)) which translate by the peaks marked with + symbol in the figure. The grain size *D* was calculated using Scherer's equation [27].

$$D = \frac{k\lambda}{\beta \cos \theta}. \quad (3)$$

Where *k* is the shape factor = 0.9, λ is the wavelength of CuK_α = 1.5406 Å, θ is the Bragg's angle and β is the full width at half maximum of diffraction peak measured in radians. Using the very intense peak (015) i.e.

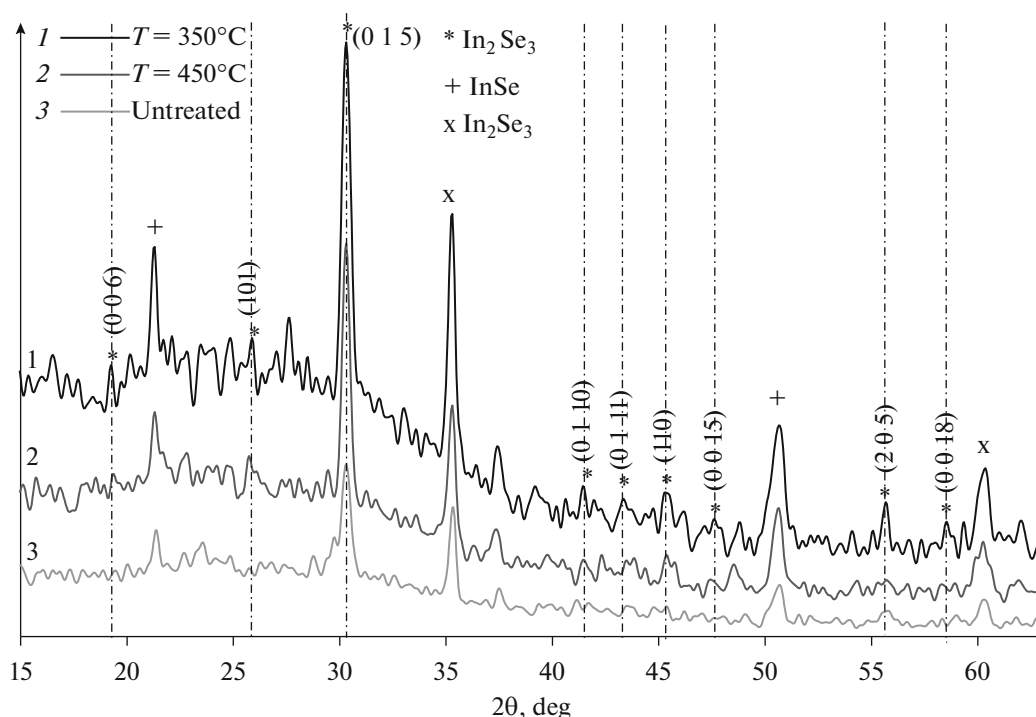


Fig. 2. X-ray spectra of electrodeposited In_2Se_3 prepared on indium tin oxide (ITO) substrate at -1.3 V vs. SCE during 10 min, annealed at different heat treatment temperatures.

the peaks at around 30.26° grain size value was obtained as $D = 9.57$ nm.

To confirm the obtained results in XRD analysis, we characterized also these three elaborated samples by RAMAN scattering spectroscopy. The Raman spectrum characteristic of electrodeposited In_2Se_3 films is shown in Fig. 3 where we can see a broad peak at 253 cm^{-1} is distinctive of the In_2Se_3 phase. The strongest feature at 253 cm^{-1} and a shoulder at 235 cm^{-1} in the Raman spectrum of In_2Se_3 film are attributed to Se_8 rings and Se_n molecules [16, 28].

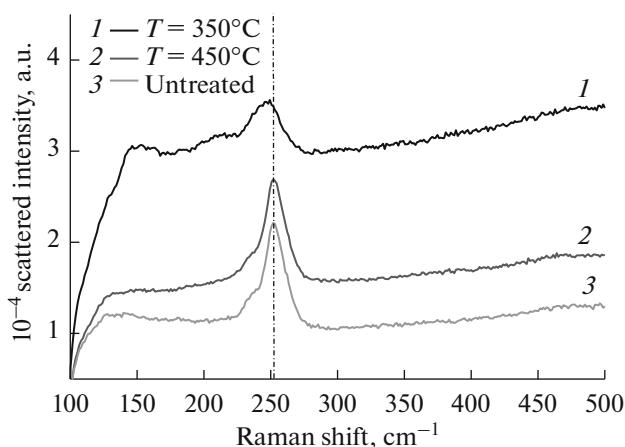


Fig. 3. Raman spectroscopy of electrodeposited In_2Se_3 prepared at -1.3 V vs. SCE during 10 min on ITO substrate, annealed at different heat treatment temperatures.

Determination of energy gap as well as the transition type of a semiconductor material can be performed using UV–Visible spectrophotometry according to the flow equation [29]:

$$ah\nu = A(h\nu - E_g)^n. \quad (4)$$

A is a constant which also depends on the refractive index of the material, the reduced mass and the light speed in the vacuum. The exponent n depends on the transition type: for a direct gap (rutile) $n = 0.5$ and for an indirect gap (anatase) $n = 2$. α is the reverse of the absorption length (the optical absorption coefficient) which is a function with the thickness d , the transmittance t and the reflection coefficient of the semiconductor R , it's given by the following formula [30–33].

$$\alpha = \frac{1}{d} \ln \left[\frac{(1-R)^2}{2t} + \left(\frac{(1-R)^4}{4t^2} + R^2 \right)^{1/2} \right]. \quad (5)$$

The transmittance spectrums UV–Visible for the electrodeposited In_2Se_3 alloy on ITO substrate at -1.3 V vs. SCE applied potential during 10 min, annealed at 350 , 450°C and untreated with the trace $(\alpha h\nu)^2$ vs. $(h\nu)$ for each sample are represented in the Fig. 4. The thicknesses of obtained films at this potential were estimated as $2\text{ }\mu\text{m}$, which were used to get the absorption coefficient values α from the transmittance values t . This figure shows that the In_2Se_3 alloys are photoactive films in the UV–Visible range, which translates by the transmission bands, the plot $(\alpha h\nu)^2$ vs. $(h\nu)$ is valid to estimate the energy gap value

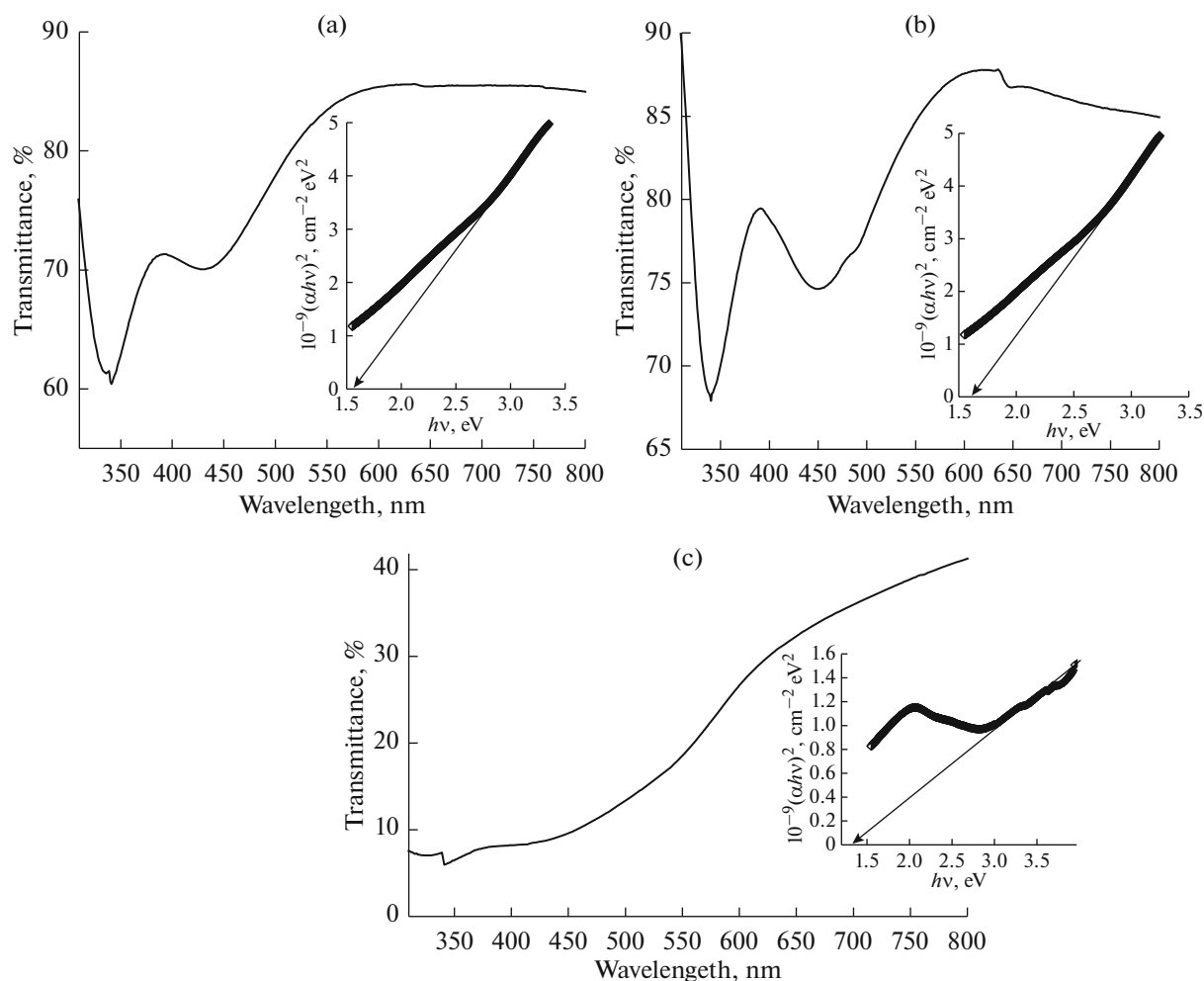


Fig. 4. Transmittance spectra with the plot $(\alpha h\nu)^2$ versus $h\nu$ of In_2Se_3 thin films electrodeposited on ITO substrates at -1.3 V vs. SCE during 10 min, (a) treated at 350°C , (b) 450°C and (c) untreated.

according to equation (4) ($n = 0.5$ for the In_2Se_3 thin layers), from this equation when $\alpha h\nu$ tends towards zero $h\nu$ tends towards E_g , which leads that extrapolation on the axis ($h\nu$) gives us directly the energy gap value, in the plotted curves extrapolation gives values of energy gap equal to $E_g = 1.55$ and 1.60 eV for the deposited In_2Se_3 treated at 350 and 450°C respectively. In the case of untreated deposit we can see that the energy gap take a small value (about 1.33 eV) compared with the annealed samples. In addition, as we can see, the plots $(\alpha h\nu)^2$ vs. $h\nu$ for the treated samples at 350 and 450°C have shapes far from the ideal shape (spectrum better aligned) this can be explained by the decrease of refractive index with the increase of heat treatment temperature, which increases relatively the value of the energy gap [34–38] and effects to the value of the constant A also. In other hand the decrease of the tensile strain in the films due to the increase of heat treatment temperature could have an impact on the increase of energy gap value [39].

Figure 5 presents the Mott–Schottky measurement of indium selenide thin films electrodeposited

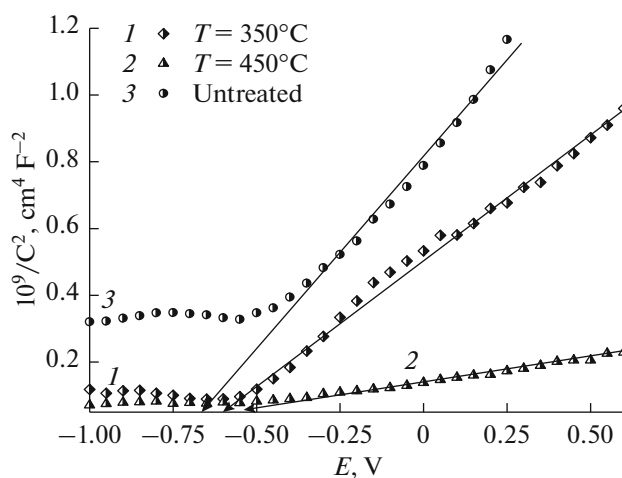


Fig. 5. Mott–Schottky plots traced in $(0.1$ M) of KCl aqueous solution with employed frequency 0.5 kHz for electrodeposited In_2Se_3 thin films at -1.3 V vs. SCE during 10 min on ITO substrate, annealed at different heat treatment temperatures.

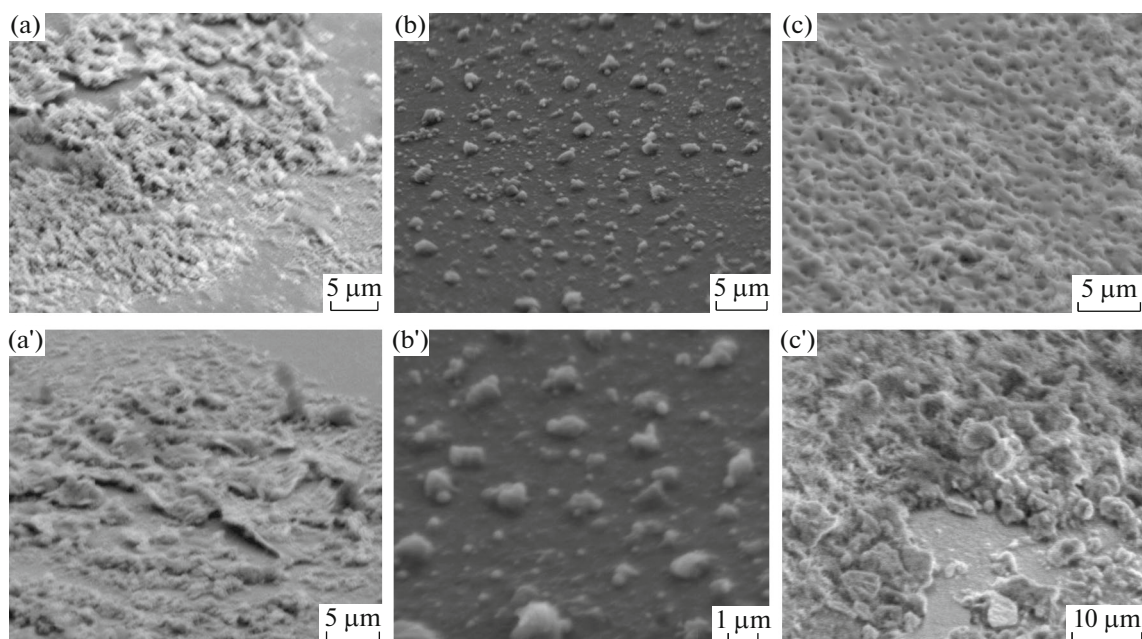


Fig. 6. SEM images of electrodeposited In_2Se_3 films on ITO substrates with applied potential -1.3 V vs. SCE during 10 min. (a, a') Annealed at 350°C , (b, b') at 450°C and (c, c') as-deposited (without heat treatment).

on ITO substrate at -1.3 V vs. SCE applied potential during 10 min examined on (0.1 M) KCl aqueous solution with employed frequency (0.5 kHz). The basis of this method is the formation of Schottky barrier between the semiconductor material and electrolytic solution [37–39]; it involves measuring the capacitance of the space charge region (C_{sc}) according to electrode potential [40]:

$$\frac{1}{C_{sc}^2} = \frac{2}{\epsilon\epsilon_0 N_d S^2} \left(E - E_{fb} - \frac{kT}{e_0} \right). \quad (6)$$

Where ϵ_0 is the space permittivity (8.85×10^{-14} F cm^{-1}), ϵ is the relative dielectric of In_2Se_3 (7.2), N_d is the concentration of the free carrier in the semiconductor, S is the area in contact with the electrolytic solution, E is the electrode potential, E_{fb} is the flat band potential, k is the Boltzmann constant (1.38×10^{-23} J K^{-1}), T is the absolute temperature (298 K), and e_0 is the charge of electron. In this figure, we can observe that the three samples exhibited positive slopes, indicating the

N -type characteristic of the (In_2Se_3) obtained semiconductor. The slope of the tangent line in Mott–Schottky plots is proportional to the $1/N_d$; also the intersection of this tangent line with the abscissa axis gives us the flat band potential. Values of flat band potential E_{fb} and concentration of free carrier N_d relating to each sample are outlined in Table 1.

SEM pictures of the three samples are presented in Fig. 6. We can see that the obtained films on each sample formed by nanosized particles, homogeneous and very dense. In the case of 350°C annealing temperature we can observe that the deposit formed is dense with very small grain size where the formed grains in the form of grass and close between them which can give a great adhesion to the formed film in this case. The annealed deposit at 450°C is less dense with spherical grains relatively big and spaced between them. In the case of as-deposited In_2Se_3 (untreated sample i.e without heat treatment); it's clear that the obtained deposit is denser compared with deposits annealed with small spherical grain size and binding in each other which leads to a good adhesion to the formed film on the substrate.

In this research, atomic force microscopy (AFM) was used also in order to investigate the surface roughness of In_2Se_3 films. AFM images of the same three samples are presented in the Fig. 7. From the 2D and 3D obtained images. We can note that the deposit treated at 350°C exhibits a relatively low surface roughness where we can say that we have very smooth surface of electrodeposited In_2Se_3 alloy (Fig. 7a). The same thing can be observed for the deposit annealed at

Table 1. Variation of flat band potential and free carrier concentration values according to the heat treatment temperature of electrodeposited In_2Se_3 thin films

Heat treatment temperature	350°C	450°C	Untreated
E_{fb} (V vs. SCE)	−0.60	−0.54	−0.66
$10^{-21} \times N_d$ (cm^{-3})	6.56	33.00	4.14

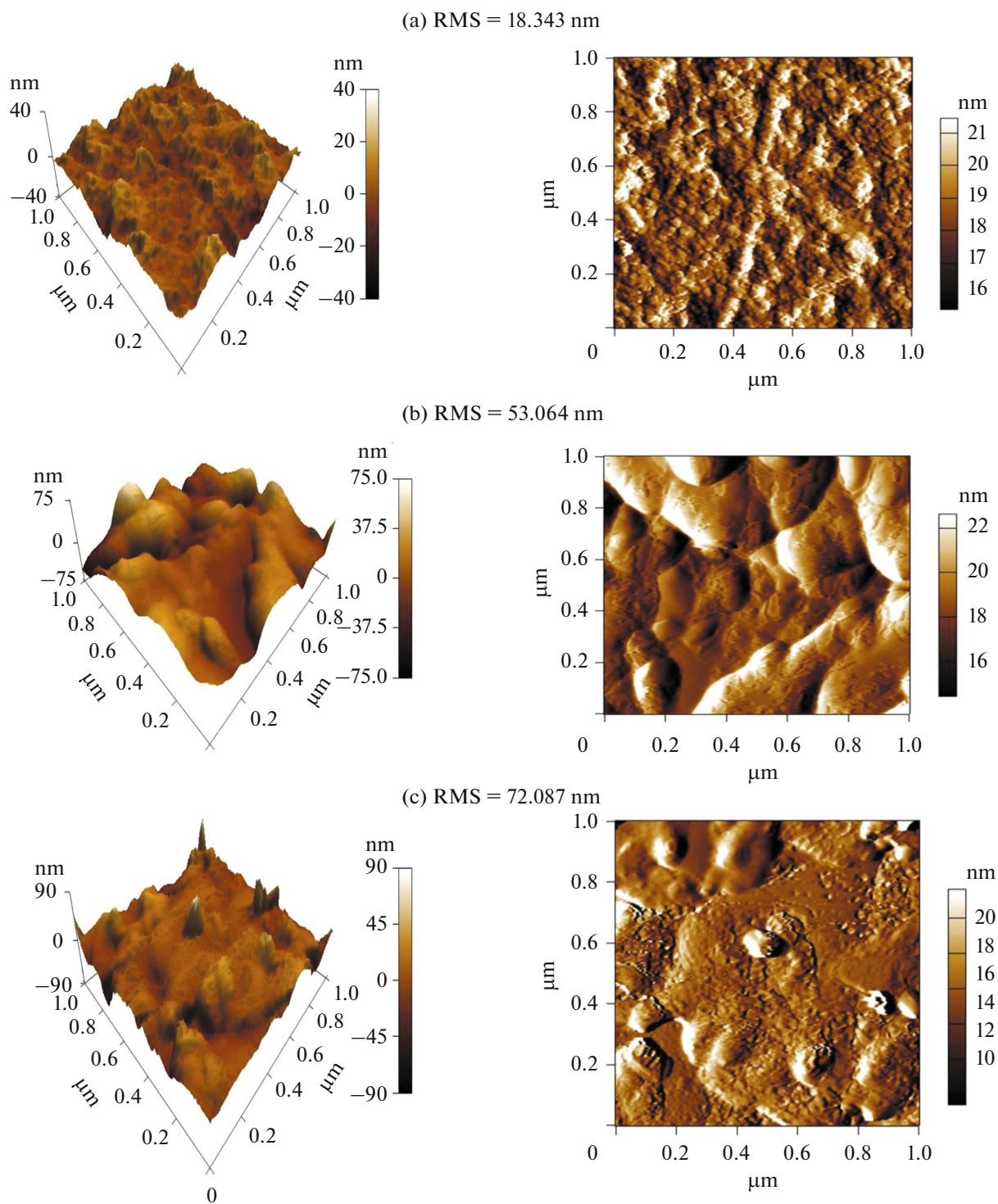


Fig. 7. AFM images of electrodeposited In_2Se_3 films on ITO substrates with applied potential -1.3 V vs. SCE during 10 min. (a) Annealed at 350°C , (b) at 450°C and (c) as-deposited (without heat treatment).

450°C with significant roughness surface compared to the previous sample (Fig. 7b). Whereas the untreated sample has a certain roughness as the (Fig. 7c) shows, this is due to the small size of the grains and fully compatible with what we saw in the SEM pictures.

Figure 8 shows the variation of root mean square (RMS) roughness of the electrodeposited In_2Se_3 thin films deposited at 1.3 V vs. SCE according to heat treatment temperature. It is found that the surface roughness is strongly dependent to annealed tempera-

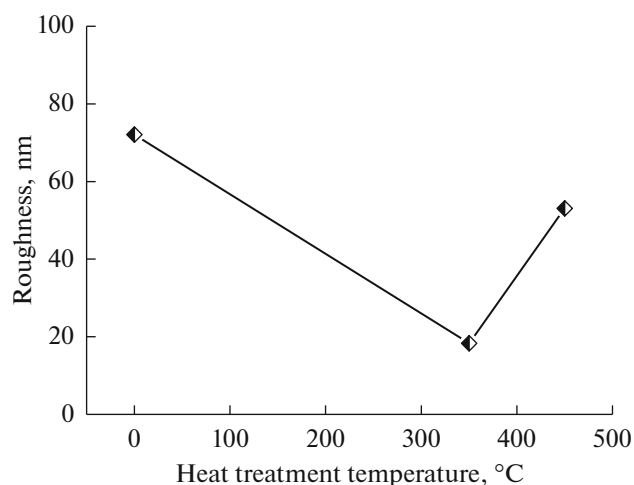


Fig. 8. Variation of the RMS roughness of electrodeposited In_2Se_3 thin films with heat treatment temperature.

ture where we can see that the maximum values of RMS roughness is in the case of untreated sample, which confirms that the thermal annealing of the electrodeposited film increases its surface smoothness due to the increase of cohesion between the grains and their fusion into each other at times, as well as the increase in their adhesion onto the surface substrate also.

CONCLUSIONS

Electrodeposition of indium selenide thin films have been studied in thin paper, obtained films were synthesized from an aqueous solution containing InCl_3 and SeO_2 in acid medium (pH 4.2) at ambient temperature using sodium citrate as complexing agent which serve to approximate the deposition potentials, synthesis process was followed by vacuum annealing of elaborated films. It was concluded that electrodeposited In_2Se_3 annealed at 350, 450°C and untreated, have the rhombohedral β -phase crystalline structure hR5. As-deposited and annealed In_2Se_3 are photoactive thin films with band-gap energies 1.33, 1.55 eV respectively and belong to n-type semiconductors with number of charge carriers in the order of $10^{21}/\text{cm}^3$ and composed mainly of In_2Se_3 nano-grains with low roughness surface.

The recorded results would help us understand the process and the good conditions for electrodeposition of In_2Se_3 thin films with nano-grains, good adhesion and smooth surface and open up prospects for research on the same axis.

ABBREVIATION LIST

E	potential
E^0	standard potential

i	current density
c	concentration
v	scan rate
D	grain size
E_g	energy gap
z	transferred electrons number
α	absorption coefficient
d	thickness
h	Planck constant
ν	frequency
t	transmittance
R	reflexing coefficient
n_R	refractive index
C_{sc}	capacitance of the space charge region
E_{fb}	flat band potential
k	Boltzmann constant
T	temperature
N_d	concentration of free carrier
S	electrode surface
ϵ_0	space permittivity
ϵ	relative dielectric
e_0	charge of electron

ACKNOWLEDGMENTS

This work was supported by the Energetic and Solid State Electrochemistry Laboratory (Ferhat Abbas-Setif 1 University-Algeria); the authors would like to thank ZAIM Keltoum and DERBAL Sabrina for their assistances.

CONFLICT OF INTERESTS

The authors declare that they have no conflict of interest.

REFERENCES

- Marsillac, S., Combout Marie, A.M., Bernede, J.C., and Conan, A., Experimental evidence of the low-temperature formation of $\gamma\text{-In}_2\text{Se}_3$ thin films obtained by a solid-state reaction, *Thin Solid Films*, 1996, vol. 288, p. 14.
- Hariskos, D., Spiering, S., and Powalla, M., Buffer layers in $\text{Cu}(\text{In,Ga})\text{Se}_2$ solar cells and modules, *Thin Solid Films*, 2005, vol. 480, p. 99.
- Gordillo, G. and Calderón, C., CIS thin film solar cells with evaporated InSe buffer layers, *Sol. Energy Mater. Sol. Cells*, 2003, vol. 77, p. 163.
- Thomas, B., Effect of in situ post-deposition annealing on the formation of $\alpha\text{-In}_2\text{Se}_3$ thin films grown by elemental evaporation, *Appl. Phys. A*, 1992, vol. 54, p. 293.
- Amory, C., Bernede, J.C., Halgand, E., and Marsillac, S., $\text{Cu}(\text{In,Ga})\text{Se}_2$ films obtained from $\gamma\text{-In}_2\text{Se}_3$ thin film, *Thin Solid Films*, 2003, vol. 431–432, p. 22.
- Li, S., Yan, Y., Zhang, Y., Ou, Y., Ji, Y., Liu, L., Yan, C., Zhao, Y., and Yu, Z., Monophase $\gamma\text{-In}_2\text{Se}_3$ thin film

- deposited by magnetron radio-frequency sputtering, *Vacuum*, 2014, vol. 99, p. 228.
7. Yan, Y., Li, S., Ji, Y., Liu, L., Yan, C., Zhang, Y., Yu, Z., and Zhao, Y., Fabrication of high-quality $\gamma\text{-In}_2\text{Se}_3$ nanostructures using magnetron sputtering, *Mater. Lett.*, 2013, vol. 109, p. 291.
 8. Bernède, J.C., Marsillac, S., and Conan A., Electrical properties of $\gamma\text{-In}_2\text{Se}_3$ layers synthesized by solid state reaction between In and Se thin films, *Mater. Chem. Phys.*, 1997, vol. 48, p. 5.
 9. Hsiang, H.I., Lu, L.H., Chang, Y.L., Ray, D., and Yen, F.S., CuInSe_2 nanocrystallite reaction kinetics using solid state reaction from Cu_2Se and In_2Se_3 powders, *J. Alloys Compd.*, 2011, vol. 509, p. 6950.
 10. Okamoto, T., Yamada, A., and Konagai, M., Growth and characterization of In_2Se_3 epitaxial films by molecular beam epitaxy, *J. Cryst. Growth*, 1997, vol. 175, p. 1045.
 11. Chang, K.J., Lahn, S.M., Xie, Z.J., Chang, J.Y., Uen, W.Y., Lu, T.U., Lin, J.H., and Lin, T.Y., The growth of single-phase In_2Se_3 by using metal organic chemical vapor deposition with AlN buffer layer, *J. Cryst. Growth*, 2007, vol. 306, p. 283.
 12. Huang, Y.C., Li, ZY., Uen, W.Y., Lan, S.M., Chang, K.J., Xie, Z.J., Chang, J.Y., Wang, S.C., and Shen, J.L., Growth of $\gamma\text{-In}_2\text{Se}_3$ films on Si substrates by metal-organic chemical vapor deposition with different temperatures, *J. Cryst. Growth*, 2008, vol. 310, p. 1679.
 13. Wei, X.F., Li, L.W., Feng, H.G., Gong, J.B., Jiang, K., and Xue, S.L., Preparation and optical properties of In_2Se_3 nanospheres using CTAB as surface modifier, *Ceram. Int.*, 2020, vol. 46, p. 1026.
 14. Simi, N.J., Vanchipurackal, and Ison, V., Structural and optical characterization of $\text{CuInS}_2\text{-In}_2\text{Se}_3$ green nanostructures synthesized by hot injection method, *Mater. Today Proc.*, 2019, vol. 8, p. 203.
 15. Wei, X., Feng, H., Li, L., Gong, J., Jiang, K., Xue, S., and Chu, P.K., Synthesis of tetragonal prismatic $\gamma\text{-In}_2\text{Se}_3$ nanostructures with predominantly {110} facets and photocatalytic degradation of tetracycline, *Appl. Catal. B*, 2020, vol. 260, p. 118218.
 16. Massaccesi, S., Sanchez, S., and Vedel, J., Electrodeposition of indium selenide In_2Se_3 , *J. Electroanal. Chem.*, 1996, vol. 412, p. 95.
 17. Valdés, M., Vázquez, M., and Goossens, A., Electrodeposition of CuInSe_2 and In_2Se_3 on flat and nanoporous TiO_2 substrates, *Electrochim. Acta*, 2008, vol. 54, p. 524.
 18. Lai, Y., Liu, F., Li, J., Zhang, Z., and Liu, Y., Nucleation and growth of selenium electrodeposition onto tin oxide electrode, *J. Electroanal. Chem.*, 2010, vol. 639, p. 187.
 19. Wang, J., Li, Q., Mu, Y., Li, S., Yang, L., Lv, P., Su, S., Liu, T., Fu, W., and Yang, H., Fabrication of CdTe thin films grown by the two-step electrodeposition technique on Ni foils, *J. Alloys Compd.*, 2015, vol. 636, p. 97.
 20. Czerniawski, J.M. and Stickney, J.L., Electrodeposition of In_2Se_3 using potential pulse atomic layer deposition, *J. Phys. Chem. C*, 2016, vol. 120, p. 16162.
 21. Herrero, J. and Ortega, J., Electrochemical synthesis of photoactive In_2Se_3 thin films, *Sol. Energy Mater.*, 1987, vol. 16, p. 477.
 22. Shi, H., Li, M., Shaygan Nia, A., Wang, M., Park, S., Zhang, Z., Lohe, R.M., Yang, S., and Feng, X., Ultrafast electrochemical synthesis of defect-free In_2Se_3 flakes for large-area optoelectronics, *Adv. Mater.*, 2020, vol. 32, p. 1907244.
 23. Pourbaix, M., *Atlas d'équilibre électrochimique à 25°C*, Gauthier-Villars et Cie, 1963.
 24. Zein El Abedin, S., Saad, A.Y., Farag, H.K., Borisenko, N., Liu, Q.X., and Endres, F., Electrodeposition of selenium, indium and copper in an air- and water-stable ionic liquid at variable temperatures, *Electrochim. Acta*, 2007, vol. 52, p. 2746.
 25. Senthikumar, M., Mathiyarasu, J., Joseph, J., Phani, K.L.N., and Yegnaraman, V., Electrochemical instability of indium tin oxide (ITO) glass in acidic pH range during cathodic polarization, *Mater. Chem. Phys.*, 2003, vol. 108, p. 403.
 26. Lutz, H. D., Fischer, M., Baldus, H.-P., and Blachnik, R., Zur polymorphie des In_2Se_3 , *J. Less-Common Met.*, 1988, vol. 143, p. 83.
 27. Jenkins, R. and Snyder, R.L., *Introduction to X-ray Powder Diffractometry*, New York: Wiley, 1996.
 28. Weszka, J., Daniel, P., Burian, A., Burian, A.M., and Nguyen, A.T., Raman scattering in In_2Se_3 and InSe_2 amorphous films, *J. Non-Cryst. Solids*, 2000, vol. 265, p. 98.
 29. Singh, R.P., Singh, S.L., and Chandra, S., Electrodeposited semiconducting CuInSe_2 films. I. Preparation, structural and electrical characterization, *J. Phys. D: Appl. Phys.*, 1986, vol. 19, p. 1299.
 30. Gonzalez-Hernandez, J., Gorley, P.M., Holrley, P.P., Vartsabyuk, O.M., and Vorobiev, Yu.V., X-ray, kinetic and optical properties of thin CuInS_2 films, *Thin Solid Films*, 2002, vol. 403-404, p. 471.
 31. Yamaguchi, T., Yamamoto, Y., Tanaka, T., Tanashi, N., and Yoshida, A., Influence of annealing temperature on the properties of Cu(In,Ga)Se_2 thin films by thermal crystallization in Se vapor, *Sol. Energy Mater. Sol. Cells*, 1998, vol. 50, p. 1.
 32. Huang, C.J., Meen, T.H., Lai, M.Y., and Chen, W.R., Formation of CuInSe_2 thin films on flexible substrates by electrodeposition (ED) technique, *Sol. Energy Mater. Sol. Cells*, 2004, vol. 82, p. 553.
 33. Sadigov, M.S., Ozkan, M., Bacaksiz, E., Altunbas, M., and Kopya, A.I., Production of CuInSe_2 thin films by a sequential processes of evaporations and selenization, *J. Mater. Sci.*, 1999, vol. 34, p. 4579.
 34. Tripathy, S.K., Refractive indices of semiconductors from energy gaps, *Opt. Mater.*, 2015, vol. 46, p. 240.
 35. El-Shair, H.T. and Bekheet, A.E., Effect of heat treatment on the optical properties of In_2Se_3 thin films, *J. Phys. D: Appl. Phys.*, 1992, vol. 25, p. 1122.
 36. Aly, S.A., El Sayed, N.Z., and Kaid, M.A., Effect of annealing on the optical properties of thermally evaporated ZnO films, *Vacuum*, 2001, vol. 61, p. 1.

37. Qasrawi, A.F., Temperature dependence of the direct allowed transitions band gap and optical constants of polycrystalline α - In_2Se_3 thin films, *Thin Solid Films*, 2006, vol. 514, p. 267.
38. El-Nahass, M.M., Saleh, A.-B.A., Darwish, A.A.A., and Bahlol, M.H., Optical properties of nanostructured InSe thin films, *Opt. Commun.*, 2012, vol. 285, p. 1221.
39. Peng, L.P., Fang, L., Yang, X.F., Li, Y.J., Huang, Q.L., Wu, F., and Kong, C.Y., Effect of annealing temperature on the structure and optical properties of In-doped ZnO thin films, *J. Alloys Compd.*, 2009, vol. 484, p. 575.
40. Rousset, J., Saucedo, E., and Lincot, D., Extrinsic doping of electrodeposited zinc oxide films by chlorine for transparent conductive oxide applications, *Chem. Mater.*, 2009, vol. 21, p. 534.
41. Windisch, C.F. and Exarhos, G.J., Mott–Schottky analysis of thin ZnO films, *J. Vac. Sci. Technol.*, 2000, vol. 18, p. 1677.
42. Mora-Sero, I., Fabregat-Santiago, F., Denier, B., Bisquert, J., Tena-Zaera, R., Elias, J., and Levy-Clement, C., Determination of carrier density of ZnO nanowires by electrochemical techniques, *Appl. Phys. Lett.*, 2006, vol. 89, p. 203117.
43. Morrison, S.R., *Electrochemistry at Semiconductor and Oxidized Metal Electrodes*, New York: Plenum Press, 1980.